

NPBDREG: A Non-parametric Bayesian Deep-Learning Based Approach for Diffeomorphic Brain MRI Registration

Samah Khawaled¹ and Moti Freiman ^{*2}

¹*Department of Applied Mathematics*

²*Department of Biomedical Engineering*

^{1,2}*Technion, Israel Institute of Technology, Haifa, Israel*

Abstract

Quantification of uncertainty in deep-neural-networks (DNN) based image registration algorithms plays an important role in the safe deployment of real-world medical applications and research-oriented processing pipelines, and in improving generalization capabilities. Currently available approaches for uncertainty estimation, including the variational encoder-decoder architecture and the inference-time dropout approach, require specific network architectures and assume parametric distribution of the latent space which may result in sub-optimal characterization of the posterior distribution for the predicted deformation-fields. We introduce the NPBDREG, a fully non-parametric Bayesian framework for unsupervised DNN-based deformable image registration by combining an Adam optimizer with stochastic gradient Langevin dynamics (SGLD) to characterize the true posterior distribution through posterior sampling. The NPBDREG provides a principled non-parametric way to characterize the true posterior distribution, thus providing improved uncertainty estimates and confidence measures in a theoretically well-founded and computationally efficient way. We demonstrated the added-value of NPBDREG, compared to the baseline probabilistic VoxelMorph unsupervised model (PrVXM), on brain MRI images registration using 390 image pairs from four publicly available databases: MGH10, CMUC12, ISBR18 and LPBA40. The NPBDREG shows a slight improvement in the registration accuracy compared to PrVXM (Dice score of 0.73 vs. 0.68, $p \ll 0.01$), a better generalization capability for data corrupted by a mixed structure noise (e.g Dice score of 0.729 vs. 0.686 for $\alpha = 0.2$) and last but foremost, a significantly better correlation of the predicted uncertainty with out-of-distribution data ($r > 0.95$ vs. $r < 0.5$).

1 Introduction

Deformable image registration is a fundamental task needed in a wide-range of magnetic resonance imaging (MRI) applications, including: motion compensation, multi-modal analysis, *inter* or *intra* subject alignment for change detection, and longitudinal analysis, to name a few [17, 35]. For a comprehensive overview of both classical and deep-neural-networks (DNN) based registration methods and their different categories we refer the reader to [30] and [16]. Classical methods formulate the ill-posed deformable registration task as a regularized optimization problem over the deformation fields space and solve it using iterative solvers [6, 8]. However, these conventional algorithms are computationally demanding, which in turn, makes the registration of a new pair of images a computationally expensive process. In light of the success of DNN-based methods in numerous computer vision tasks, several studies aimed to propose more efficient and less time-consuming deformable registration

approaches based on DNN models [11, 9, 2, 34, 28, 32]. These techniques learn a deformation field prediction model either through a supervised learning framework (i.e with the help of provided reference deformation fields) [34] or in an unsupervised manner [9, 2, 32]. The latter is advantageous as it doesn't require reference deformation fields. Instead, such unsupervised DNN models are trained to predict the deformation field from a given pair of template (fixed) and moving input images by using some dissimilarity measure between the images as the loss function.

However, the practical utilization of DNN-based image registration methods in clinical applications is hampered by the lack of computational mechanisms for quantifying the risks of failure in their predictions. For example, Fig. 1 depicts two cases of success and failure of the network to predict the correct deformation field without a noticeable difference in the input images. Mechanisms to determine the prediction's confidence by estimating the uncertainty of the DNN prediction play a critical role in adopting DNN-based methods for safety-critical clinical applications such as MRI analysis and reconstruction as the resulting outputs inform

^{*}is a Taub fellow (supported by the Taub Family Foundation, Technion's program for leaders in Science and Technology)

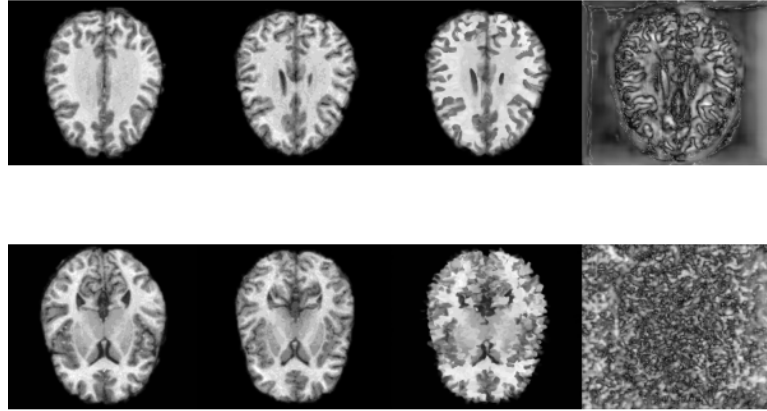


Figure 1: Importance of uncertainty assessment in registration of brain MRI image to a given template. From left to right: Brain MRI image, fixed template, the resulting warped image and the voxel-wise uncertainty map. The first row presents an example in which the DNN predicted a deformation field that successfully mapped the patient data onto the template data (mean value of uncertainty is 2.179) while the second row presents a failure of the DNN to predict the deformation field (mean value of uncertainty is 2.69).

diagnostic, prognostic, and interventional decisions in medicine and scientific conclusions in research [31, 4].

Bayesian DNN-based models can enable safer utilization in medical imaging, improve generalization, and assess the uncertainty of the predictions by characterizing the entire posterior distribution of the network parameters. Recently, two main methods were proposed to assess the uncertainty in DNN-based methods for tasks in MRI such as image registration [3, 34], analysis in diffusion MRI [31], and MRI reconstruction from under-sampled data [13]. The approaches include inference-time dropout [19] and variational encoder-decoder models [21]. Yang et al. [34] extend their supervised predictive model to a probabilistic version by repeating the inference for a specific data sample multiple times while maintaining stochastic dropout layers. At each repetition, the dropout layers randomly set some of the network units to 0. The voxel-wise variance of the outputs can then be used as an estimate of the uncertainty in the predictions. From a practical perspective this method is simple and efficient, yet it lacks flexibility since it can be used only on DNN-based methods that trained with dropout layers and cannot be generalized to any DNN architecture. Further, from a theoretical perspective, it may not fully express a meaningful uncertainty estimate that is associated with the network predictions [18]. Specifically, Osband [25] demonstrated that an inference-time dropout estimation of uncertainty does not negatively correlate with adding more data to the training process as expected from an uncertainty measure of DNN predictions.

Recently, Dalca et al. proposed a probabilistic VoxelMorph DNN for image registration [2, 3], where uncertainty estimates are obtained with a variational encoder-decoder model. This approach

relies on a probabilistic generative model, which computes an approximate posterior distribution, $q_\theta(z|X)$, where z is a velocity field generated by the encoder-decoder model. q is constrained by a prior distribution, $p(z)$, which is assumed to be a normal distribution. The modeling of z as a Gaussian distribution is done by adding a Kullback-Leibler (KL) divergence term, $KL(p||q)$, to the loss function used to train the DNN. This approach, however, is limited to specific DNN architectures. Further, it assumes a parametric distribution of the latent space in the form of a Gaussian distribution which may represent an oversimplification of the unknown true underlying distribution.

In a shift from previous approaches, we propose a new, non-parametric, Bayesian approach for Diffeomorphic registration (NPBDREG) of brain MRI images, which provides an uncertainty assessment of the predictions. We adopt the strategy of stochastic gradient Langevin dynamics (SGLD) [33] to perform the sampling from the posterior distribution of the network weights [10]. Specifically, we inject Gaussian noise to the loss gradients during the training phase of our framework, and keep all weights obtained after the “burn-in” iteration.¹ We estimate the posterior distribution of the deformation field during inference by averaging deformation field predictions obtained by the model with the saved weights. Our approach does not make any prior assumptions about the underlying distribution and can be applied to any DNN architecture,

¹Following the notation of SGLD [33], the *burn-in* phase is the initial stage of SGLD learning, at which the step size is still relatively large, thus the gradients magnitude dominates the injected noise. After this phase, the step size decays, thus, the injected Gaussian noise will dominate the loss behavior as its curve converges and exhibits only small variations around its steady-state.

without the need to introduce additional stochastic layers such as the dropout layer or modeling the latent distribution through mean and variance layers. Further it can be adjoined to most DNN training schemes, either supervised or unsupervised.

The remainder of this paper is organized as follows: section 2 provides a general background on image registration. Then, we introduce the proposed NPBDREG method in section 3. Section 4 describes the metric used to evaluate the registration performance and the measure that quantifies the voxel-wise uncertainty. Section 5 discusses the experiments performed on brain MRI images, and lastly, section 6 concludes our work and discusses open questions and possible future studies.

2 Background: Image Registration

Registration is the process of mapping a pair of images (e.g. MR images acquired from different subjects) onto one coordinate system. Registration models can be loosely characterized by two categories of spatial transformations: *global* and *local*. The former is related to the rigid family, where an image is translated or rotated, or to the affine transformations, which perform shear mapping and scaling, in addition to rotation and translation. However, the latter accounts for non-linear dense transformations, or spatially varying (non-uniform) deformation models [30]. Local deformations can be modeled by various geometric, physical, and interpolation models (e.g. the cubic B-splines model [27]), for more details we refer an interested reader to [15, 30].

Deformable registration can be formulated as an optimization problem. Let us denote the pair of fixed and moving images by I_f and I_M , respectively. Φ is the deformation field, which accounts for mapping the grid of I_M to the grid of I_f . Then, the energy functional that we aim to optimize is:

$$\arg \min_{\Phi} S(I_f, I_M \circ \Phi) + \lambda R(\Phi) \quad (1)$$

where $I_M \circ \Phi$ denotes the result of warping the moving image with Φ . S is a dissimilarity term, which quantifies the resemblance between the resulting image and the fixed input, and R is a regularization term that encourages the deformation smoothness. The scalar λ is a tuning-parameter that accounts for balancing the two terms, and it controls the smoothness of the resulted deformation.

In DNN-based registration, the task of the model is to predict the deformation: $\Phi = f_{\theta}(I_M, I_F)$, where θ are the parameters of the network and I_M, I_F are the input pairs. It should be emphasized that, in contrast to supervised schemes, unsupervised registration models “learn” the deformation field that maps from I_M to I_F without providing a reference transformation. In the case of non-

parametric (free-form) deformation,² it predicts Φ by optimizing the following:

$$\hat{\theta} = \arg \min_{\theta} S(I_F, I_M \circ f_{\theta}(I_M, I_F)) + \lambda R(f_{\theta}(I_M, I_F)) \quad (2)$$

This kind of optimization provides the best point-estimate of network parameters, θ , that is the solution of Maximum Likelihood estimation (MLE).

Bayesian DNN-based models have the potential to characterize the entire posterior distribution of the network parameters [23, 10]:

$$P(\theta | I_M, I_F) = \frac{P(I_M, I_F | \theta) P(\theta)}{\int_{\Theta} P(I_M, I_F | \theta') P(\theta') d\theta'} \quad (3)$$

Since direct integration of the posterior distribution is intractable, it is common to assume either a general or a domain-specific formulation of the prior $P(\theta)$ such as a Gaussian distribution with $\mu = 0$ on the network parameters and aimed to maximize the posterior estimation of the prediction:

$$\hat{\theta} = \arg \max_{\theta} P(\theta | I_M, I_F) \propto P(I_M, I_F | \theta) P(\theta) \quad (4)$$

While this can provide a maximum-a-posterior (MAP) point estimation of the DNN output, it cannot characterize the entire distribution of the output, which is necessary to assess confidence in the DNN prediction.

3 The NPBDREG Approach

To address this challenge, we use an SGLD mechanism [33] to characterize the actual posterior distribution of the model weights as follows. We treat the network weights as random variables and aim to sample the posterior distribution of the model prediction. To this end, we incorporate a noise scheduler that injects a time-dependent Gaussian noise to the gradients of the loss during the optimization process. At every training iteration, we add Gaussian noise with *adaptive* variance to the loss gradients. Then, the weights are updated in the next iteration according to the “noisy” gradients. This noise schedule can be performed with any stochastic optimization algorithm during the training procedure. In this work we focused on the formulation of the method for the `Adam` optimizer. We use Gaussian noise with a variance proportional to the learning rate of the `Adam` optimization algorithm, as it allows the adaption of the noise to the nature of loss curve. Moreover, previous research shows better performance using noise adaptive or time-dependent variance than constant variance [24]. Our SGLD-based registration NPBDREG method is outlined in algorithm 1.

²Here, we don’t consider the parametric or model-based deformation (such as affine-based or spline-based) and we limit the discussion to the free-form only. In the parametric case, the network predicts the parameters of the deformation.

Algorithm 1: NPBDREG Algorithm

Input: Tuning parameters λ and α , and number of epochs N
Output: Estimated deformation $\hat{\Phi}$ and registered image I_R
Data: Dataset of pairs of fixed and moving images I_M, I_F

/* The *offline* training */

1 **Function** TrainNetwork($I_M, I_F, \lambda, \alpha^t, N$):

2 **for** $t < N$ **do**

3 Compute loss, L^t , for validation and training sets $\tilde{g}^t \leftarrow g^t + \mathbf{N}^t$, where $\mathbf{N}^t \sim \mathcal{N}(0, \frac{s^t}{\alpha^t})$ and s^t is the *adaptive* step size.

4 $\theta^{t+1} \leftarrow \text{ADAM_UPDATE}(\theta^t, \tilde{g}^t)$

5 **end**

6 **return** $\{\theta^t\}_{t_b}^N, \{L^t\}_{t_b}^N$

/* *Online* Registration */

1 **Function**

2 FeedForward($I_M, I_F, \{\theta_t\}_{t_b}^N, \{w^t\}_{t_b}^N$):

3 Compute a set of velocity fields $\{V^t\}_{t_b}^N$ by feed-forwarding I_M , $V^t = f_{\theta^t}(I_M, I_F)$ for $t \in [t_b, N]$

4 Estimate the weighted mean:

5 $\hat{V} = \frac{\sum_{t=t_b}^N w^t V^t}{\sum_{t=t_b}^N w^t}$

6 $\Sigma_v \leftarrow$ The variance of \hat{V} given $\{V^t\}_{t_b}^N$

7 Calculate the diffeomorphic deformation: $\Phi \leftarrow \text{INT_LAYER}(I_{in}, \hat{V})$

8 Register image: $I_R \leftarrow \text{SPATIAL_TRANSFORM}(I_{in}, \Phi)$.

9 **return** I_R, Φ, Σ_v

3.1 Offline Training

$L(I_M, I_F, f_{\theta}(I_M, I_F))$ denotes the overall registration loss, described in (2), which is composed of both similarity and regularization terms. We denote the loss gradients by:

$$g^t \triangleq \nabla_{\theta} L^t(I_M, I_F, f_{\theta}(I_M, I_F)) \quad (5)$$

where t is the training iteration (epoch). At each training iteration, Gaussian noise with time-varying variance is added to g :

$$\tilde{g}^t \leftarrow g^t + \mathbf{N}^t \quad (6)$$

where $\mathbf{N}^t \sim \mathcal{N}(0, \frac{s^t}{\alpha^t})$, s^t is the **Adam** step size, and α^t is a user-selected parameter that controls the noise variance (can be time-decaying or a constant). This is especially important in the first learning stages, which involve a large step size. The network parameters are then updated according to the **Adam** update rule:

$$\theta^{t+1} \leftarrow \theta^t - s^t \hat{m}^t \quad (7)$$

where $s^t = \frac{\eta}{\sqrt{\hat{v}^t + \epsilon}}$, \hat{m}^t and \hat{v}^t are the bias-corrected versions of the decaying averages of the past gradients and the second moment (squared gradients),

respectively:

$$\begin{aligned} \hat{m}^t &= m^t / 1 - \beta_1^t \\ \hat{v}^t &= v^t / 1 - \beta_2^t \end{aligned} \quad (8)$$

where $m^t = m^{t-1} + (1 - \beta_1) \tilde{g}^t$ and $v^t = v^{t-1} + (1 - \beta_2) (\tilde{g}^t)^2$. β_1, β_2 are decay rates and η is a fixed constant.

3.2 The Registration System

Our main building-block is a UNet-based [26] convolutional network (CNN) similar to the Probabilistic VoxelMorph model [2], followed by an integration layer, which is responsible for the diffeomorphism of the deformation. Fig. 2 illustrates the operation of NPBDREG on a pair of fixed and moving images. Having the network trained, and its weights during training saved, we exploit only the outputs of the network with weights obtained after the *burn-in* phase. We sample a set of velocity fields $\{V^t\}_{t_b}^N$, obtained by feed-forwarding the pairs I_M, I_F to our UNet after the *burn-in* phase. t_b denotes the cut-off point of the *burn-in* phase and N is the iterations number. Under some feasible constraints on the step size, the sampled weights converge to the posterior distribution [33] (See A for further discussion). Thus, outputs of our network after the *burn-in* phase, trained with the *adaptive* SGLD approach can be considered as a sampling from the true posterior distribution.

Then, when we have a new pair for alignment, we estimate the averaged posterior velocity field:

$$\hat{V} = \frac{\sum_{t=t_b}^N w^t V^t}{\sum_{t=t_b}^N w^t} \quad (9)$$

where w_t is a predetermined weight parameter. To give a larger weight to networks with better performance, w^t is proportional to the total loss calculated on the validation set, at epoch t . This is due to the fact that the loss is negative, where local-cross-correlation (LCC) was used as a dissimilarity loss. In addition, we quantify the voxel-wise uncertainty maps of the registration by means of empirical variance of the velocity fields, Σ_V . A further description of uncertainty assessment is mentioned in subsection 4.5. A numerical integration, using scaling and squaring (briefly outlined in subsection 3.3), operates on the averaged velocity field, \hat{V} , to yield a diffeomorphic deformation, Φ . Lastly, we register the moving image by resampling its coordinate system with the spatial transform Φ . The function SPATIAL_TRANSFORM performs spatial warping. For each voxel p , a sub-voxel location $\Phi(p)$ is calculated. Then, the values are linearly interpolated to obtain an integer.

Uncertainty Estimation Uncertainty of DNN models can be loosely classified into two types: Aleatoric and Epistemic [19]. The former is caused by noise in the data (for example, noise added to

the input images), whereas, the latter is induced by an uncertainty in the parameters of the model. In DNN frameworks, Bayesian methods aims to quantify the Epistemic uncertainty by characterizing the posterior predictive distribution. As such, our NPBDREG system provides a voxel-wise Epistemic uncertainty map of the registration by Monte Carlo sampling from the posterior of our network, which trained with the SGGLD-based strategy. Particularly, we sample a set of velocity fields from models with weights obtained in iterations t_b, \dots, N , $\{V_t\}_{t_b}^N$, we then calculate the voxel-wise diagonal covariance (variance), Σ_V . Finally, the uncertainty of the velocity field can be calculated by:

$$H_V = \frac{1}{2} \log(2\pi\Sigma_V) \quad (10)$$

By the same manner, one may quantitatively assess the uncertainty of the registration field where Σ_V in (10) is replaced by the diagonal covariance calculated over the set of Diffeomorphic Deformations obtained by *scaling of squaring* each $\{V_t\}_{t_b}^N$.

Architecture and Training Our main UNet-based building block is comprised from an encoder and decoder with skip connections, as highlighted in Fig. 3. Both encoder and decoder parts consist of CNN layers with kernel size $3 \times 3 \times 3$, followed by Leaky ReLU activation functions. The encoder has 4 CNN layers, each with $\{16, 32, 32, 32\}$ channels, whereas, the decoder consists of 5 layers with the following number of channels: $\{32, 32, 32, 32, 16\}$. Afterwards, a 3-channel convolutional layer is applied on the UNet output to obtain the 3D deformation field. The training process of the model involves the optimization of the energy-functional described in (2). We use LCC for our MRI images experiments to characterize the dissimilarity between the fixed image I_F and that obtained after mapping, $I_M \circ \hat{\Phi}$. The L_2 norm over the deformation field gradients is used as a regularization term to encourage the deformation field smoothness. The UNet model then learns the optimal weights by minimizing the loss function composed of the two aforementioned terms.

3.3 Integration method

Diffeomorphic deformation is a differentiable and invertible transformation, $\Phi : \mathbb{R}^3 \rightarrow \mathbb{R}^3$, which maps the coordinates from the moving image to the fixed image. Similarly to [2], we consider a stationary velocity field representation, where the deformation field is defined through the following ODE:

$$\begin{cases} \frac{\partial \Phi^{(t)}}{\partial t} = V(\Phi^{(t)}) \\ \Phi^{(0)} = I \end{cases} \quad (11)$$

where V is the the deformation field and I is the identity transformation. Then, We obtain Φ by integrating the stationary velocity field, v , over $t =$

$[0, 1]$. The solution of the ODE (11) is characterized by an exponential of V , that is $\Phi^{(1)} = \exp(V)$. In our implementation we adopt the *Scaling and Squaring* method to compute the matrix exponential efficiently [5]. The *scaling and squaring* scheme can be outlined in the following steps:

1. **Scaling step:** $V(x) \leftarrow \frac{V(x)}{2^T}$
where $\frac{V(x)}{2^T}$ is sufficiently small (desired accuracy according to predetermined T , we refer to T as the integration steps)
2. **Exponentiation step:** $\Phi^{\frac{1}{2^T}} \leftarrow V(x)$ (first-order explicit scheme)
3. **Squaring step:** Perform T recursive squarings of $\Phi^{\frac{1}{2^T}}$
loop over $t = \{T, \dots, 1\}$: $\Phi^{\frac{1}{2^{t-1}}} \leftarrow \Phi^{\frac{1}{2^t}} \circ \Phi^{\frac{1}{2^t}}$

The intuitive interpretation of this method is that the deformation at time $T = 1$ is given as a result of 2^T times the composition of the small deformations obtained at time $1/2^T$. For further details about this method refer to [5].

4 Experimental Methodology

4.1 Database and Preprocessing

T1-weighted MRI images of the brain for 80 subjects were acquired from four different database sources: MGH10, CMUC12, ISBR18 and LPBA40.³ MGH10 consists of the brain MRI images of 10 subjects, with atlases of segmentations divided into 74 manually labeled regions. The images were inhomogeneity-corrected and affine-registered to the MNI152 template. CMUC12 includes MRIs of 12 subjects with atlases of 128 labeled regions. The images were rotated into cardinal orientation. ISBR18 consists of T1-weighted MRI image data of 18 subjects and their segmentations were divided into 84 individual anatomical structures. Images were processed by autoseg bias field correction. LPBA40⁴ have whole-head MRI images of 40 subjects with manual delineations of 56 structures [29]. Images were preprocessed according to existing protocols to produce skull-stripped brain volumes. All images were multiplied by their provided brain masks, zero-padded to size of $256 \times 256 \times 256$, resampled to a uniform grid and size $(1 \times 1 \times 1)$, then cropped to the central $160 \times 192 \times 224$, and normalized to the $[0, 1]$ gray-scale domain. Further, affine alignment was performed using *dipy* library, which maximizes the mutual information (MI) via optimization strategy similar to ANTS [7]. We Split each dataset into: training, evaluation, and test sets with the following ratios: 56%, 30% and 14%, respectively. Then, we constructed 292, 20 and 78

³used in <https://continuousregistration.grand-challenge.org/data/> and in [22] (with a detailed description about each database.)

⁴are available at <http://www.loni.ucla.edu/Atlases/LPBA40>

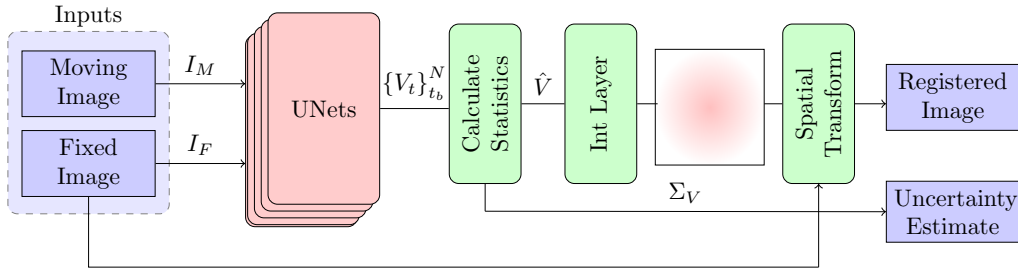


Figure 2: Block diagram of the proposed NPBDREG system. After having a set of velocity fields, $\{V_t\}_{t_b}^N$, we calculate the averaged fields and the voxel-wise variance, \hat{V} and Σ_V , respectively. Only the average is used in the registration scheme, but, Σ_V is utilized for uncertainty assessment.

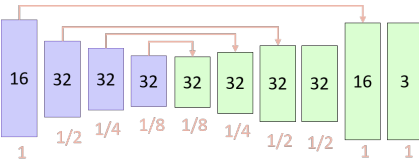


Figure 3: The UNet Architecture. Arrows represent skip connections between the corresponding layers.

pairs from each dataset for training, evaluation, and testing, respectively.

4.2 Implementation details

We implemented our NPBDREG method for brain MRI images using Keras with a tensorflow backend [1].⁵ The NPBDREG network was trained with noise injections for 4,000 iterations. We used an Adam optimizer [20] of learning rate which was set to 2^{-4} and added a L_2 regularization of network weights and biases to our loss function to avoid overfitting. We empirically set the L_2 regularization weight to 10^{-7} and the total integration steps to, $T = 6$. We used exhaustive search to determine the best value for the smoothness parameter, λ which provides best performance in terms of both registration accuracy and smoothness of the deformation fields. Additionally, we trained the NPBDREG with two configurations: (1) a fixed α^t , the std of the noise injected to the gradients was set to $s^t = lr/50$. (2) a time-decaying α^t , the std of the noise injected to the gradients was set to $s^t = lr/(1+t)^{0.55}$. At inference time, our model registers a new pair I_F and I_M onto one coordinate system by resampling with the mean transformation Φ , yielded by averaging deformations obtained in the last 8 iterations. We used the probabilistic VoxelMorph (PrVXM) model [2] as a baseline for the purpose of performance comparison in terms of registration accuracy and uncertainty quantification. We trained PrVXM with the same optimizer and settings but without gradient noise injections; a UNet architecture identical to NPBDREG was

	$ J_\Phi < 0$		Dice	
	mean	std	mean	std
$\lambda = 0.005$	0.028	0.0041	0.7252	0.0541
$\lambda = 0.01$	0.021	0.0034	0.7349	0.0541
$\lambda = 0.1$	0.014	0.0023	0.7394	0.0537
PrVXM	0.017	0.0043	0.6882	0.0657

Table 1: Percentages of folds and Dice score for different values of λ . The mean and std values of percentage of folds and dice score, calculated over the whole test set, for the deformation fields obtained by NPBDREG with three values of λ , $\lambda = \{0.005, 0.01, 0.1\}$ and the baseline PrVXM. The number of folds i.e. voxels with negative determinant of the Jacobian, $|J_\Phi| < 0$, is computed. Then, the percentage of folds for each volume is calculated by dividing the total number of folds by the overall number of voxels. The best dice score and minimal number of folds are obtained by the model with $\lambda = 0.1$.

used.

4.3 Evaluation of registration accuracy

We evaluated the performance of our Bayesian unsupervised registration system by means of a Dice score [12, 2]. The Dice score measures the registration accuracy by quantifying the volume overlap between a reference segmentation and the propagated (registered) structure:

$$D = 2 \frac{P \cap R}{P \cup R} \quad (12)$$

where P and R are the propagated and reference labels, respectively. The Dice score varies in the range $[0, 1]$, a Dice score of 1 implies identical structures and complete overlap achieved by perfect registration, while a Dice score of 0 implies no overlap between the sets. We selected 6 labels of anatomical structures, provided by the atlases to evaluate the registration performance by means of Dice score as follows: initial Dice score after affine alignment was calculated for all labels in the atlases, then, only 6 labels with the largest volume size and a Dice

⁵source code of NPBDREG, which includes the training algorithm and preprocessing scripts will be published upon acceptance.

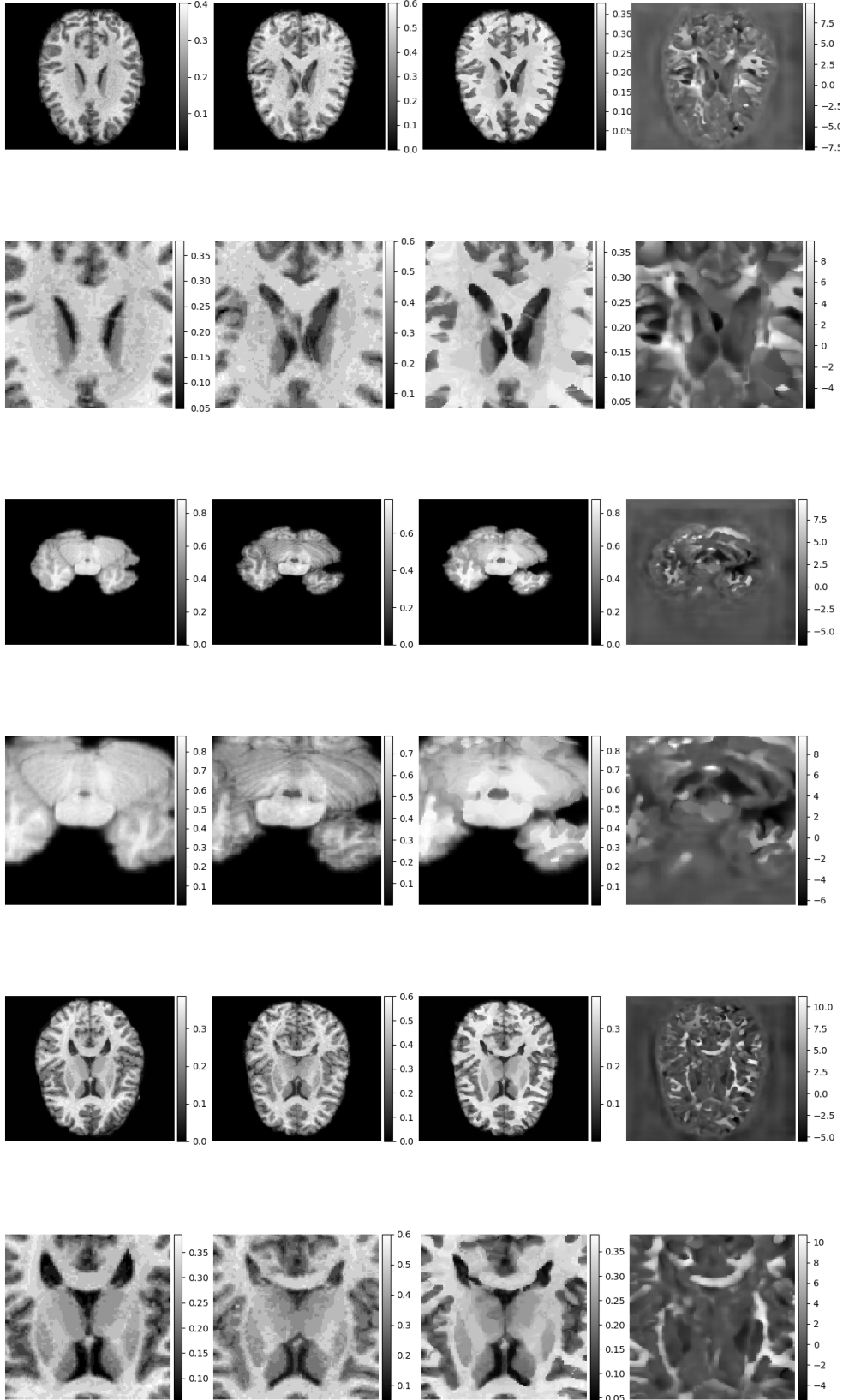


Figure 4: Registration results. Rows 1, 3 and 5: examples of MRI slices of input moving image, fixed image, and resulting warped image and the corresponding deformation field (from left to right). The observed images belong to MGH10 and LPBA40 database sources, respectively. Rows 2, 4 and 6: closeups of the center regions of the moving, fixed and registered images, and the registration field, respectively.

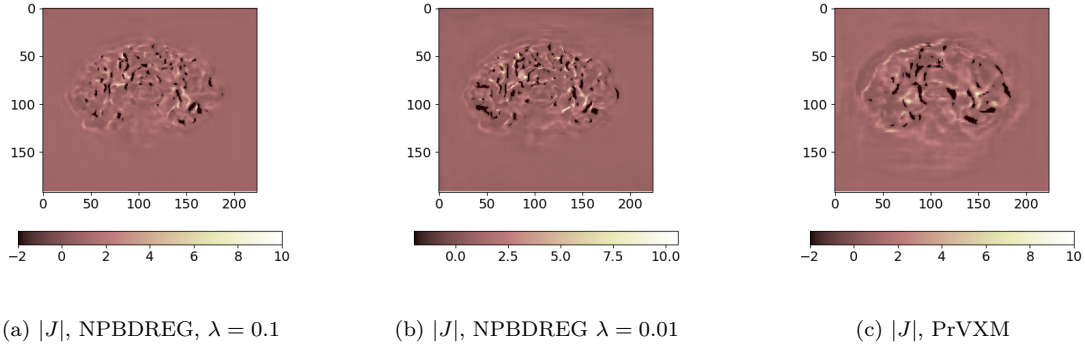


Figure 5: Hot maps of the Jacobian determinant of the deformation field, $|J|$, obtained by NPBDREG with $\lambda = 0.1$ (a), NPBDREG with $\lambda = 0.01$ (b) and PrVXM (b). The percentage of folds for each example of the aforementioned deformations are: 0.013, 0.019 and 0.015, respectively. The percentage of folds for each volume is calculated by dividing the total number of folds by the overall number of voxels.

Method	MGH10	CUMC12	ISBR18	LPBA40
NPBDREG (1)	0.798	0.0101	0.7302	0.0407
NPBDREG (2)	0.790	0.0089	0.721	0.0484
PrVXM	0.797	0.0107	0.629	0.0628

Table 2: Evaluation results. The mean and std of Dice metric, calculated over labels and test examples for each database (columns), are presented for the three different models (from top to bottom: NPBDREG with configurations (1) and (2) and the baseline PrVXM, respectively.

score bigger than 0.5 were selected and used in our experiments. The anatomical labels used for Dice calculations are presented in Table 4 (See C).

4.4 Improved generalization capability

We analyzed the improvement in DNN-based registration generalization capabilities achieved by our NPBDREG approach. We corrupted the input images with two types of noise: Gaussian noise with various std (σ) and mixed structures, which generated a linear combination of the test example (i) and another example sampled randomly from the test set (j): $\alpha I_j + (1 - \alpha) I_i$ [14]. We used the Dice score and the same labels as in the previous experiment to determine the added-value of our NPBDREG approach in increasing generalization capabilities of the registration system.

4.5 Uncertainty Assessment

We assessed the capability of our NPBDREG approach to characterize uncertainty related to out-of-distribution data. We randomly selected a group of 8 images from the test set. We simulated out of distribution data by corrupting the images with Gaussian noise with varying σ_n . We computed the empirical voxel-wise diagonal covariance (variance), Σ_V as follows: We sampled 8 deformations, one from each of the networks with weights obtained in the last 8 iterations. Then, we computed the uncertainty in the velocity field as mentioned in (10). Finally we assessed the correlation between the computed uncertainty and the noise levels (σ_n).

5 Experimental Results

Fig. 4 presents several registration results of our NPBDREG system. Table 1 presents the registration results of the NPBDREG model for 3 different values of λ . We assessed the effect of the parameter λ on both the registration accuracy and the smoothness of the deformation. Further, we compared the performance of our method and the baseline PrVXM [2]. We quantified the registration accuracy by computing the mean values of Dice score on the test set, averaged over the different anatomical labels. In addition, we assessed the smoothness of the predicted deformation fields by calculating the percentage of folds, i.e. voxels with negative determinant of the Jacobian, $|J_\Phi| < 0$. We selected the model with the value of λ that optimized both the number of folds and dice score. Hence and henceforth, we use NPBDREG system with $\lambda = 0.1$.

Evaluation via Dice Averaged values of Dice metrics, over the anatomical labels, are calculated for each one of the different datasets (Table 2). We observed, both NPBDREG with configurations (1) and (2) achieved (on average) significant improvements over PrVXM in terms of Dice metric (we conducted a paired t-test with $p \ll 0.01$ on the test set).⁶ In addition, the nature of α^t , which tunes the std of the gradients' noise, doesn't have a significant effect on the registration accuracy, i.e. both fixed and time-decaying α^t yielded approximately similar performances (paired t-test with $p = 0.093 > 0.01$). Thus, in the following analysis and experiments we

⁶ p denotes the calculated P value

Method	Gaussian				Mixed Structure			
	$\sigma = 0$	$\sigma = 0.4$	$\sigma = 0.6$		$\alpha = 0.2$	$\alpha = 0.4$		
NPBDREG (1)	0.739	0.0537	0.702	0.0568	0.682	0.0566	0.729	0.0563
NPBDREG (2)	0.723	0.0541	0.698	0.0548	0.681	0.0555	0.716	0.0558
PrVXM	0.688	0.0657	0.687	0.0619	0.679	0.0623	0.686	0.0640

Table 3: Evaluation results. The added noise levels are denoted by σ and α , respectively. The mean and std of the Dice metric, calculated over the whole test set and over labels, are presented for the three different models (from top to bottom: NPBDREG with configurations (1) and (2) and the baseline PrVXM, respectively.

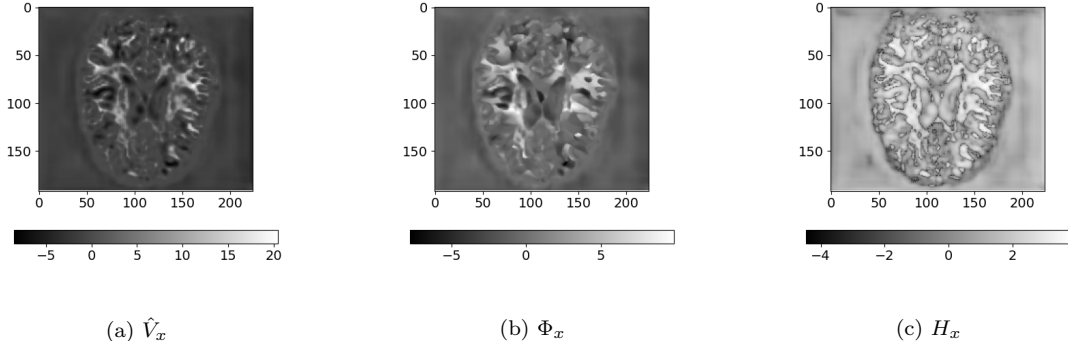


Figure 6: Uncertainty assessment. (a) and (b) The averaged velocity field and the corresponding deformation in x direction, respectively. (c) uncertainty maps of the deformation in x direction, H_x .

consider only NPBDREG (1), where α^t is fixed. Table 3 summarizes the quantitative results obtained by NPBDREG with the two configurations and PrVXM, for different noise levels σ and α . NPBDREG shows a significant improvement over PrVXM in noisy scenarios ($p \ll 0.01$). One may note that the accuracies of registration obtained by our method and PrVXM are similar for the MGH10 database. In our evaluation experiments, only a few examples from MGH10 were selected in the test set, since this source includes only 10 subjects.

Aleatoric Uncertainty with Registration An example of a voxel-wise uncertainty map is observed in Fig. 6. Fig. 7 depicts the correlation between the measure of uncertainty and the level of data corruption by noise. We measured the correlation between the two variables by computing the Pearson correlation coefficient, r . The high correlation ($r = 0.96$, $p < 10^{-4}$) indicates the ability of the NPBDREG uncertainty measures to detect out-of-distribution data that would result in unreliable DNN predictions. The out-of-distribution data was generated by adding an increasing amount of noise to the pairs of MRI data serving as the registration DNN-based input.

6 Conclusions

In this paper we developed a non-parametric Bayesian DNN-based method for deformable MRI registration. We used noise injection to the training loss gradients to efficiently sample the true posterior distribution of the network weights. Our proposed

approach formulated the training mechanism for an **Adam** optimizer, however, it can be directly extended to other stochastic optimization algorithms as well.

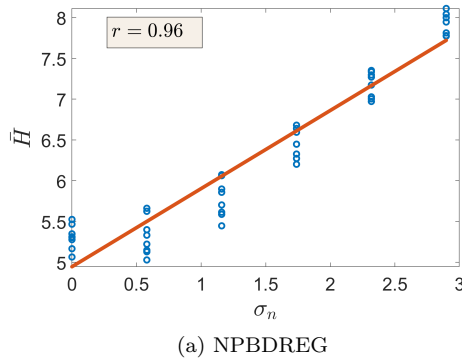
The proposed approach provides empirical estimates of the two principle moments of the deformation field, which, in turn, can be directly employed to assess the uncertainty in the deformation field. In addition, other statistics or higher-order moments can be empirically calculated from the posterior samples. Our experiments showed that a non-parametric Bayesian DNN-based registration with posterior sampling through gradient noise injection shows a slight improvement on the registration accuracy by means of a Dice score, both in noisy and non-noisy scenarios, compared to the point estimates predicted by the Probabilistic VoxelMorph model. Further, it provides an uncertainty measures that correlates with the out-of-distribution data.

acknowledgments

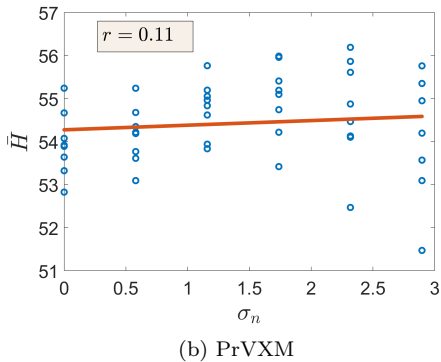
Khawaled, S. is a fellow of the Ariane de Rothschild Women Doctoral Program.

References

- [1] Martién Abadi et al. “Tensorflow: Large-scale machine learning on heterogeneous distributed systems”. In: *arXiv preprint arXiv:1603.04467* (2016).



(a) NPBDREG



(b) PrVXM

Figure 7: Correlation between the NPBDREG and PrVXM estimate of uncertainty and out-of-distribution data. (a) and (b) Scatter plots of the mean value of uncertainty estimate, \bar{H} , of NPBDREG and PrVXM versus the amount of noise added to the input images, σ_n . In contrast with PrVXM, the uncertainty measure of NPBDREG exhibits a high correlation with the noise level ($r > 0.95$). r denotes the computed Pearson correlation coefficient.

[2] Adrian V. Dalca et al. “Unsupervised Learning for Fast Probabilistic Diffeomorphic Registration”. In: *MICCAI: Medical Image Computing and Computer Assisted Intervention, LNCS 11070* (2018), pp. 729–738.

[3] Adrian V. Dalca et al. “Unsupervised Learning of Probabilistic Diffeomorphic Registration for Images and Surfaces”. In: *Medical Image Analysis* 57 (2019), pp. 226–236.

[4] Vegard Antun et al. “On instabilities of deep learning in image reconstruction—Does AI come at a cost?” In: *arXiv preprint arXiv:1902.05300* (2019).

[5] Vincent Arsigny et al. “A log-euclidean framework for statistics on diffeomorphisms”. In: *International Conference on Medical Image Computing and Computer-Assisted Intervention*. Springer. 2006, pp. 924–931.

[6] John Ashburner. “A fast diffeomorphic image registration algorithm”. In: *Neuroimage* 38.1 (2007), pp. 95–113.

[7] Brian B Avants et al. “A reproducible evaluation of ANTs similarity metric performance in brain image registration”. In: *Neuroimage* 54.3 (2011), pp. 2033–2044.

[8] Brian B Avants et al. “Symmetric diffeomorphic image registration with cross-correlation: evaluating automated labeling of elderly and neurodegenerative brain”. In: *Medical image analysis* 12.1 (2008), pp. 26–41.

[9] Guha Balakrishnan et al. “An unsupervised learning model for deformable medical image registration”. In: *Proceedings of the IEEE conference on computer vision and pattern recognition*. 2018, pp. 9252–9260.

[10] Zezhou Cheng et al. “A bayesian perspective on the deep image prior”. In: *Proceedings of the IEEE Conference on Computer Vision and Pattern Recognition*. 2019, pp. 5443–5451.

[11] Adrian Dalca et al. “Learning conditional deformable templates with convolutional networks”. In: *Advances in neural information processing systems*. 2019, pp. 804–816.

[12] Lee R Dice. “Measures of the amount of eco-logic association between species”. In: *Ecology* 26.3 (1945), pp. 297–302.

[13] Vineet Edupuganti et al. “Uncertainty quantification in deep mri reconstruction”. In: *IEEE Transactions on Medical Imaging* 40.1 (2020), pp. 239–250.

[14] Moti Freiman, Ravindra Manjeshwar, and Li-ran Goshen. “Unsupervised abnormality detection through mixed structure regularization (MSR) in deep sparse autoencoders”. In: *Medical physics* 46.5 (2019), pp. 2223–2231.

[15] Eldad Haber and Jan Modersitzki. “Numerical methods for volume preserving image registration”. In: *Inverse problems* 20.5 (2004), p. 1621.

[16] Grant Haskins, Uwe Kruger, and Pingkun Yan. “Deep learning in medical image registration: A survey”. In: *Machine Vision and Applications* 31.1 (2020), p. 8.

[17] Derek LG Hill et al. “Medical image registration”. In: *Physics in medicine & biology* 46.3 (2001), R1.

[18] Laurent Valentin Jospin et al. “Hands-on Bayesian Neural Networks—a Tutorial for Deep Learning Users”. In: *arXiv preprint arXiv:2007.06823* (2020).

[19] Alex Kendall and Yarin Gal. “What uncertainties do we need in bayesian deep learning for computer vision?” In: *arXiv preprint arXiv:1703.04977* (2017).

[20] Diederik P Kingma and Jimmy Ba. “Adam: A method for stochastic optimization”. In: *arXiv preprint arXiv:1412.6980* (2014).

[21] Diederik P Kingma and Max Welling. “Auto-encoding variational bayes”. In: *arXiv preprint arXiv:1312.6114* (2013).

- [22] Arno Klein et al. “Evaluation of 14 non-linear deformation algorithms applied to human brain MRI registration”. In: *Neuroimage* 46.3 (2009), pp. 786–802.
- [23] Radford M Neal. *Bayesian learning for neural networks*. Vol. 118. Springer Science & Business Media, 2012.
- [24] Arvind Neelakantan et al. “Adding gradient noise improves learning for very deep networks”. In: *arXiv preprint arXiv:1511.06807* (2015).
- [25] Ian Osband et al. “Deep exploration via bootstrapped DQN”. In: *arXiv preprint arXiv:1602.04621* (2016).
- [26] Olaf Ronneberger, Philipp Fischer, and Thomas Brox. “U-net: Convolutional networks for biomedical image segmentation”. In: *International Conference on Medical image computing and computer-assisted intervention*. Springer, 2015, pp. 234–241.
- [27] Daniel Rueckert et al. “Nonrigid registration using free-form deformations: application to breast MR images”. In: *IEEE transactions on medical imaging* 18.8 (1999), pp. 712–721.
- [28] Wei Shao et al. “ProsRegNet: a deep learning framework for registration of MRI and histopathology images of the prostate”. In: *Medical image analysis* 68 (2021), p. 101919.
- [29] David W Shattuck et al. “Construction of a 3D probabilistic atlas of human cortical structures”. In: *Neuroimage* 39.3 (2008), pp. 1064–1080.
- [30] Aristeidis Sotiras, Christos Davatzikos, and Nikos Paragios. “Deformable medical image registration: A survey”. In: *IEEE transactions on medical imaging* 32.7 (2013), pp. 1153–1190.
- [31] Ryutaro Tanno et al. “Uncertainty modelling in deep learning for safer neuroimage enhancement: Demonstration in diffusion MRI”. In: *NeuroImage* 225 (2021), p. 117366.
- [32] Bob D de Vos et al. “A deep learning framework for unsupervised affine and deformable image registration”. In: *Medical image analysis* 52 (2019), pp. 128–143.
- [33] Max Welling and Yee W Teh. “Bayesian learning via stochastic gradient Langevin dynamics”. In: *Proceedings of the 28th international conference on machine learning (ICML-11)*. 2011, pp. 681–688.
- [34] Xiao Yang et al. “Quicksilver: Fast predictive image registration—a deep learning approach”. In: *NeuroImage* 158 (2017), pp. 378–396.
- [35] Barbara Zitova and Jan Flusser. “Image registration methods: a survey”. In: *Image and vision computing* 21.11 (2003), pp. 977–1000.

A Convergence Analysis

The sampled model parameters, θ^t , converge to the posterior distribution when $t \rightarrow \infty$, i.e. $\mathbb{E}[\theta^t] \xrightarrow{t \rightarrow \infty} \mathbb{E}[\theta]$. Therefore, the mean velocity field, calculated by averaging the velocity field samples obtained by the model, $\hat{V} = \frac{\sum_{t_b}^N w^t V^t}{\sum_{t_b}^N w^t}$, is also unbiased when $t \rightarrow \infty$ (consistent). According to SGLD [33], convergence to a local minima is guaranteed when the following requirements on the step size are accomplished:

$$\begin{cases} \sum_{t=1}^{\infty} \epsilon^t = \infty \\ \sum_{t=1}^{\infty} (\epsilon^t)^2 < \infty \end{cases} \quad (13)$$

Typical step sizes decay polynomially: $\epsilon^t = \frac{a}{(b+t)^\gamma}$ when $\gamma \in (0.5, 1]$. In our NPBDREG training, we use the **Adam** step size, denoted by s^t , and we select a proper step size that satisfies the SGLD converges. Here we provide a condition on the step size that meets the requirements mentioned in (13).

Converges Condition in NPBDREG scheme

Let s^t and ϵ^t denote the **Adam** and SGLD step sizes, respectively. The former can be written as $s^t = \frac{\eta}{\sqrt{v^t/1-\beta_2^t+\epsilon}}$, where β_2^t is the decay rate, which can be either fixed or varying with training iterations. Here we assume that ϵ^t is related to the aforementioned polynomially decaying functions. To fulfill the constraints in (13), the following should be accomplished: $s^t \in \Omega(\epsilon^t)$, i.e. there exist some constants c_1 and c_2 such that $c_1 \frac{a}{(b+t)^\gamma} \leq s^t \leq c_2 \frac{a}{(b+t)^\gamma}$. The latter yields to the following two conditions on η and β_2^t :

$$\begin{cases} \eta^2(1 - \beta_2^t) \leq v^t c_1^2 \frac{a^2}{(b+t)^{2\gamma}} \\ \eta^2(1 - \beta_2^t) \geq v^t c_2^2 \frac{a^2}{(b+t)^{2\gamma}} \end{cases} \quad (14)$$

In others words, the aforementioned requirements imply that $\beta_2^t \in \Omega\left(\frac{v^t}{(b+t)^{2\gamma}}\right)$.

B Output Statistics

In [10], it is proved that a CNN with random parameters, which is fed by a stationary input image (such as white noise), acts as a spatial Gaussian process with a stationary kernel. This is valid in the limit as the channels number in each layer goes to infinity. In addition, the authors analyze the network statistical behavior for models with beyond two layers or with more complex systems that incorporate down-sampling, sampling or skip connection. Similar to these conclusions, the deformation obtained by a CNN model with random parameters that operates on stationary pair of images behaves like a Gaussian field. We assume that the network parameters, θ are Gaussian. In our *adaptive* learning setting, the

latter is accomplished under the assumption of negligible second order moment of **Adam**, v^t , i.e. when $\beta_2 \simeq 1$.

C Anatomical Regions

Database	Labels
MGH10	L temporal pole, R temporal pole, R occipital cortex, L occipital cortex, L frontal pole, R frontal pole
CUMC12	R Cerebral White Matter, L Putamen, L Thalamus Proper, R Putamen, Brain Stem, R Thalamus Proper
ISBR18	R Frontal pole, R Supracalcarine cortex, L Intracalcarine cortex, R Intracalcarine cortex, L Supracalcarine cortex, L Frontal pole
LPBA40	L middle orbitofrontal G, R precentral G, L precentral G, L lateral orbitofrontal G, R middle orbitofrontal G, R inferior frontal G

Table 4: Anatomical regions used for Dice calculation for each one of the databases. R and L denotes right and left, respectively.